

Ternary Ni–Cu–OH and Ni–Co–OH electrodes for electrochemical energy storage

Nuha A. Alhebshi¹ · H. N. Alshareef¹

Received: 15 June 2015 / Accepted: 14 October 2015 / Published online: 28 October 2015
© The Author(s) 2015. This article is published with open access at Springerlink.com

Abstract In this project, Ni–Cu–OH and Ni–Co–OH ternary electrodes have been prepared. Different Ni:Cu and Ni:Co ratios were deposited by chemical bath deposition (CBD) at room temperature on carbon microfibers. Since Ni(OH)₂ is notorious for poor cycling stability, the goal of the work was to determine if doping with Cu or Co could improve Ni(OH)₂ cycling stability performance and conductivity against reaction with electrolyte. It is observed that the electrodes with Ni:Cu and Ni:Co composition ratio of 100:10 result in the optimum capacitance and cycling stability in both Ni–Cu–OH and Ni–Co–OH electrodes. This improvement in cycling stability can be attributed to the higher redox reversibility as indicated by the smaller CV redox peak separation. In addition, it is found that decreasing Cu and Co ratios, with fixed CBD time, enhances nanoflakes formation, and hence increases electrode capacitance. For the optimum composition (Ni:Co = 100:10), composites of the ternary electrodes with graphene and carbon nanofibers were also tested, with resultant improvement in potential window, equivalent series resistance, areal capacitance and cycling stability.

Keywords Nickel hydroxide · Graphene · Electrochemical supercapacitors

Electronic supplementary material The online version of this article (doi:10.1007/s40243-015-0064-7) contains supplementary material, which is available to authorized users.

✉ H. N. Alshareef
husam.alshareef@kaust.edu.sa

¹ Materials Science and Engineering Program, Physical Science and Engineering Division, King Abdullah University of Science and Technology (KAUST), Thuwal 23955-6900, Saudi Arabia

Introduction

The demand for electrical energy storage devices, batteries and electrochemical supercapacitors is rapidly increasing in many crucial applications such as portable electronics, electric transportation, and renewable energy systems [1]. It is well-known that rechargeable batteries have higher energy but less power than those of electrochemical supercapacitors [2]. Electrochemical supercapacitors can be classified into electrical double-layer capacitors (EDLC) and Faradic capacitors. In EDLC, charges are held at the interfacial double layer between a porous material and an electrolyte solution, while charges are stored in Faradic capacitors during Faradic oxidation–reduction (redox) reactions depending upon the electrode potential [2]. Due to the differences in these energy storage mechanisms, Faradic capacitors fundamentally exhibit higher capacitance but weaker charge–discharge cycling stability than those of ELDC. Porous materials with electrical conductivity have been earlier investigated for both fundamental understanding and practical implementations in EDLC [3, 4]. For Faradic capacitors and rechargeable batteries, transition metal oxides/hydroxides and intrinsically conductive polymers have been intensively reported in the literature [5–9].

Nickel hydroxide (Ni(OH)₂) nanomaterial is one of the most promising electrode materials for Faradic capacitors and rechargeable alkaline batteries, due to significant electrochemical redox reactivity [10], larger specific surface area than that of Ni(OH)₂ bulk material, natural abundance, environmental friendliness, and low cost. However, the main issue of Ni(OH)₂ electrodes is the capacitance decay during charge–discharge (CD) cycling. For instance, a high specific capacitance, 2222 F/g at 1 A/g, has been achieved using Ni(OH)₂ electrode prepared by chemical bath deposition (CBD) on nickel foam at room

temperature, but with a capacitance retention of 62 % after only 2000 CD cycles at 1 A/g [11]. It has been reported in the same study that the major contributor to such capacitance decay is the phase transformation from α -Ni(OH)₂ or γ -NiOOH to β -Ni(OH)₂ or β -NiOOH phases, at relatively low discharge current densities [11].

Such problem of low charge–discharge cycling stability has long been recognized for rechargeable Ni/Cd and Ni/MH alkaline batteries, and has been tackled by means of using metal additives such as Co, Ca, Zn and Al [12–16]. Co-additive results in a good electrode material for electrochemical supercapacitors because its oxides and hydroxides exhibit high capacitance, while Cu offers excellent electrical conductivity. Recently, metal additives, binary and ternary oxides/hydroxides have been used in Ni-based electrochemical supercapacitors to enhance the cycling stability, electrical conductivity and capacitance. Even though enhanced performances of Ni-based electrochemical supercapacitors have been reported in the literature, many of the synthetic processes used in electrode materials preparation are energy consuming, environmentally unfriendly, and costly. For instance, a cell-capacitance retention of 94.5 % after 4000 CD cycles at 5 A/g and a cell capacitance retention of 86 % after 47,000 CD cycles at 25 A/g have been reported for (Ni–Co–Cu)(OH)₂–CuO//AC asymmetric supercapacitor. However, its cell capacitance of \sim 58 F/g at 5 A/g and \sim 54 F/g at 25 A/g was relatively low, and it was prepared by cathodic deposition which requires external energy source [17].

In contrast to electrodeposition and hydrothermal synthesis methods, chemical bath deposition (CBD) is a highly recommended synthesis method for industrial and commercial implementations because it is simple, scalable, fast, cost effective, does not require external energy source, and can be done at room temperature. Ni(OH)₂ and NiO thin films were prepared by CBD for the first time by Pramanik and Bhattacharya [18]. Since then, Ni(OH)₂ nanomaterials prepared by CBD have been investigated and utilized as electrodes for electrochemical supercapacitors. For example, a specific capacitance of 1416 F/g at 1 A/g has been reported for conformal coating of Ni(OH)₂ nanoflakes electrode, prepared by CBD at room temperature on carbon microfibers, with a capacitance retention of 66 % after 10,000 CD cycles at 20 A/g [19]. In addition, Ni-based electrodes with metal additives, binary, and ternary hydroxides have been prepared by CBD and used in electrochemical supercapacitors. A specific capacitance of 1030 F/g at 3 A/g has been reported for Ni–Co binary hydroxides electrode, prepared by CBD at 80 °C on nickel foam, but its cycling stability was studied for only 1000 CD cycles at 15 A/g [20]. Specific capacitances of 1970 F/g at 5 mV/s and 859 F/g at 6 A/g have been reported for Ni–Cu spherical double hydroxide electrode, prepared by CBD at

room temperature on Nickel foam, but with a capacitance retention of 69 % after only 1600 CD cycles at 6 A/g [21].

Reduced graphene oxide (rGO) nanosheets have been also utilized for electrochemical supercapacitors with much better cycling stability than that of metal oxide and hydroxide electrodes [3]. One of the best results for reduced graphene oxide supercapacitors was reported by Bai et al. [22] using a modified Hummer's method and hydrothermal reduction, and obtaining a full-cell specific capacitance of 230 F/g at 1 A/g and a capacitance retention of \sim 89 % after 10,000 cycles. However, there are other simpler methods which can be used to prepare graphene, and it is useful to study their performance. One such simple method is the chemical exfoliation of graphite [23]. Chemical exfoliation is an environmentally friendly and cost-effective method as it does not require strong acids (as in Hummer's method), or high temperature and high pressure (as in the hydrothermal method). In addition, it can produce large quantity of electrically conductive graphene since it is exfoliated directly from graphite without forming graphene oxide. An et al. [23] have reported a full-cell specific capacitance of 120 F/g at 2 mA for chemically exfoliated graphene-based supercapacitors.

In this project, Ni–Cu–OH and Ni–Co–OH electrodes have been prepared using different Ni:Cu and Ni:Co ratios by CBD at room temperature on carbon microfibers. Effects of changing Ni:Cu and Ni:Co ratios on electrode morphology and electrochemical performance are investigated. For the optimum composition (Ni:Co = 100:10), composites of the ternary electrodes with graphene and carbon nanofibers were also tested, with resultant improvement in potential window, equivalent series resistance, areal capacitance and cycling stability.

Experiments

Electrode preparation

Ni–Cu–OH electrodes were prepared by CBD with Ni:Cu ratios of 100:3, 100:10 and 100:25. The chemical bath consisted of 1 M of nickel(II) sulfate hexahydrate (NiSO₄·6H₂O), different molarities (0.03, 0.10 and 0.25 M) of copper(II) sulfate pentahydrate (CuSO₄·5H₂O) and deionized (DI) water (H₂O) in Pyrex beakers at room temperature. Then, 1.56 mL of ammonium hydroxide solution (30–33 % NH₃ in H₂O) and 0.15 M of potassium persulfate (K₂S₂O₈) were added subsequently to the mixture. Several pieces of commercial carbon microfibers substrates from Fuel Cell Store (carbon cloth 7302003, 99 % carbon content and 11.5 mg/cm²) were immersed in the chemical bath by clamps at room temperature. The immersed parts of all carbon substrates have the same area

of 1.00 cm^2 . After 1 h, the coated substrates were taken out, washed several times with DI H_2O and dried in air at room temperature overnight. Ni–Co–OH electrodes with Ni:Co ratios of 100:3, 100:10 and 100:25 were prepared by the same previous procedures but with cobalt(II) chloride hexahydrate ($\text{CoCl}_2 \cdot 6\text{H}_2\text{O}$) of different molarities (0.03, 0.10 and 0.25 M). All the chemicals used in this project are of analytical grade (SIGMA-ALDRICH) and were used without further purification.

Graphene and carbon nanofibers (G-CNF) were prepared using a modified chemical exfoliation process [23]. A mixture of 100 mg of graphite and 16.5 mg of 1-pyrenecarboxylic acid (PCA) in 50 mL of methanol were sonicated for 45 min (BRANSON Ultrasonic Cleaner 2510). Then, 200 mL of DI H_2O was added to the mixture with continuous sonication for several hours. G-CNF were collected by vacuum filtration using nanoporous membranes (Celgard 3501). The collected G-CNF were dissolved in ethanol and casted drop by drop on carbon microfibers substrate at 60°C followed by washing with DI H_2O several times and drying in air overnight. Finally, G-CNF on carbon microfibers were used as substrates in CBD of the same previous procedure of Ni–Co–OH with Ni:Co ratio of 100:10 and deposition time of 1 h–2 h to prepare Ni–Co–OH/G-CNF electrodes.

Electrode characterizations

The mass loading of each electrode was calculated by weighing the carbon substrate before and after the CBD using a sensitive microbalance from METTLER TOLEDO (XP26, 0.001 mg resolution). The morphology of Ni–Cu–OH, Ni–Co–OH and Ni–Co–OH/G-CNF electrodes were observed by scanning electron microscopy (SEM) at different magnifications. The elemental spectra and mapping distribution in Ni–Cu–OH and Ni–Co–OH electrodes are confirmed by energy dispersive X-ray spectroscopy (EDX). SEM was equipped with EDX from FEI Company (Nova Nano SEM 630). G-CNF was characterized using X-ray diffraction (XRD) from Bruker Corporation (A D8 Advance System) and Raman spectroscopy from HORIBA Scientific.

Electrode performance

Ni–Cu–OH, Ni–Co–OH and Ni–Co–OH/G-CNF were used as working electrodes. Saturated calomel electrode (SCE) and a platinum (Pt) wire were used as reference electrode and counter-electrode, respectively. The aqueous electrolyte solution was 1 M of potassium hydroxide (KOH). Electrochemical redox reactions were studied by cyclic voltammetry (CV). Electrode capacitances and cycling stability were calculated by chronopotentiometric (galvanostatic) charge–discharge (CD). Equivalent series

resistances, charge transfer resistances and diffusion control were studied by electrochemical impedance spectroscopy (EIS). All experiments were carried out in standard three electrode configuration using a multi-channel Potentiostat/Galvanostat/EIS from BioLogic Science Instruments (VMP3).

Results and discussion

Elemental and morphological properties

EDX elemental mapping images for Ni–Cu–OH electrode and Ni–Co–OH electrode with Ni:Cu and Ni:Co ratios of 100:10 are shown in Fig. 1a, b, respectively. Figure 1a confirms the presence of carbon, nickel, copper and oxygen in Ni–Cu–OH electrode. In addition, it can be seen that nickel, copper and oxygen are homogeneously distributed around carbon microfibers. Figure 1b confirms the presence of carbon, nickel, cobalt and oxygen on Ni–Co–OH electrode with homogenous distribution around carbon microfibers. EDX spectra of all Ni–Cu–OH and Ni–Co–OH electrodes of composition 100:3, 100:10 and 100:25 are shown in Figure 1S (of the Supplementary Information).

SEM images in Fig. 2a–c show the morphology changes for Ni–Cu–OH electrodes of 100:3, 100:10 and 100:25, respectively. Nanoflakes are clearly shown at Ni:Cu ratio of 100:3 in Fig. 2a, while increasing the Cu content to 100:10 and 100:25 leads to suppression of nanoflake formation and to growth of flat morphology, as shown in Fig. 2b, c. SEM images Ni–Co–OH electrode of 100:3, 100:10 and 100:25 in Fig. 2d–f, respectively, show nanoflakes morphology at different stages of growth. It seems that nanoflakes in Fig. 2f have grown incompletely. It can be concluded that increasing Co ratio to 100:10 and 100:25 slows nanoflake formation and growth, even though the CBD time was fixed for all studied electrode compositions. Nanoflake morphology is considered as one of the most preferred morphologies for electrochemical supercapacitors due to the large possible interface between nanoflake surface and electrolyte. Therefore, it is expected that the nanoflake morphology, such as in Fig. 2a, d and e, leads to higher capacitance than the flat morphology, such as in Fig. 2b, c and f. Small magnification SEM images of all Ni–Cu–OH and Ni–Co–OH electrodes of 100:3, 100:10 and 100:25 are shown in Figure 2S (a)–(f) in the Supplementary Information which shows that the carbon microfibers substrates have been conformally coated. Graphene and carbon nanofibers (G-CNF) can be seen clearly in Fig. 2g. The diameter of an individual CNF is around 200 nm as shown in Figure 2S (g) in the Supplementary Information. Figure 2h shows Ni–Co–OH coated on G-CNF using Ni:Co ratio of 100:10 and a deposition time

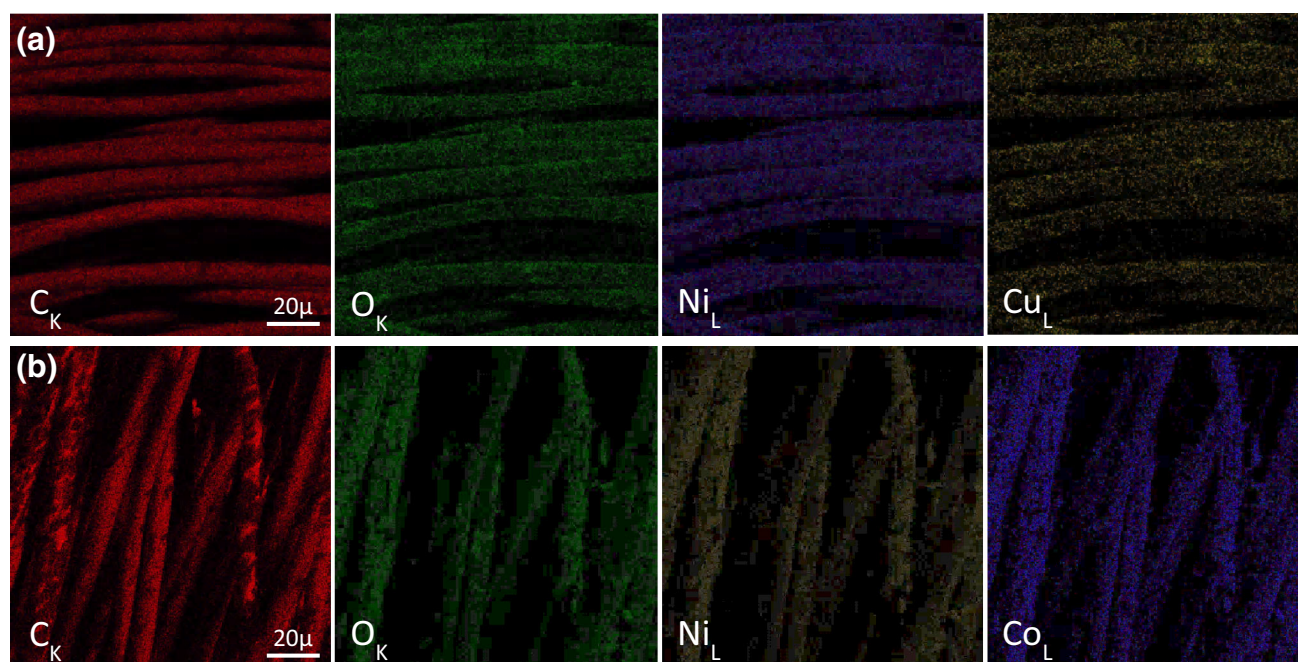


Fig. 1 a, b EDX elemental mapping images for Ni–Cu–OH and Ni–Co–OH electrodes, respectively

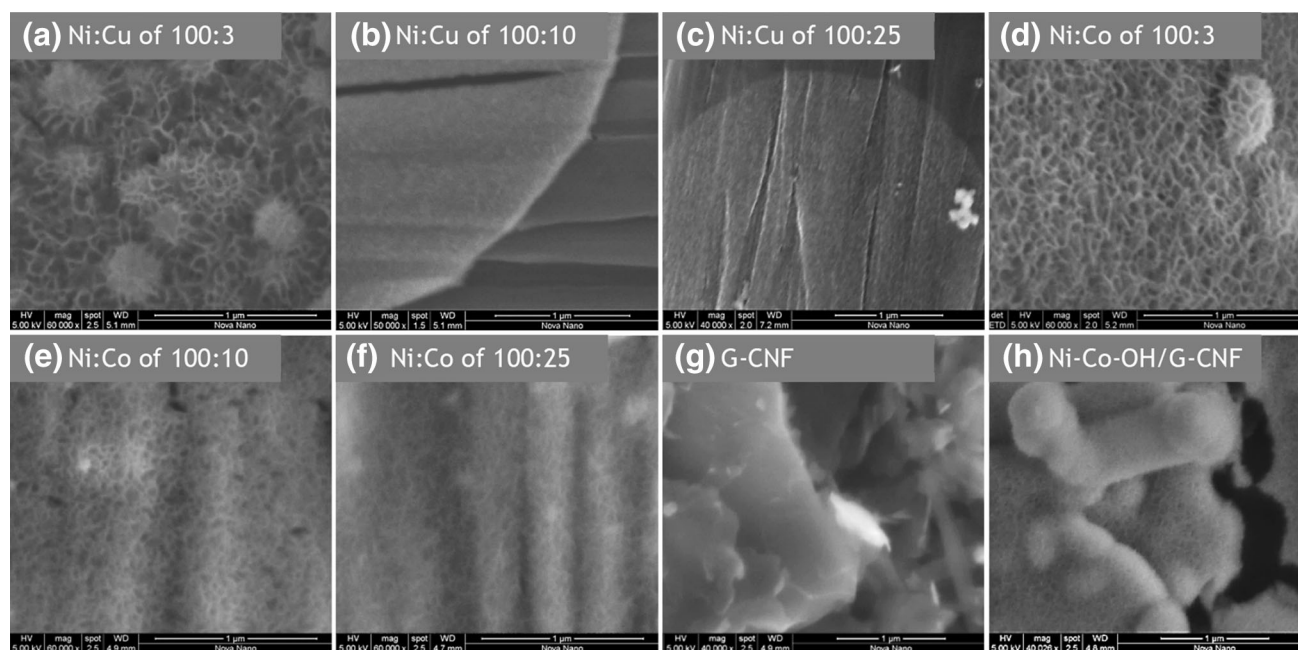


Fig. 2 SEM images of a–c Ni–Cu–OH electrodes of 100:3, 100:10 and 100:25, respectively. d–f Ni–Co–OH electrodes of 100:3, 100:10 and 100:25, respectively. g G–CNF electrode. h Ni–Co–OH/G–CNF electrode. All electrodes are coated on carbon microfibers substrates

of 1 h. Using the same ratio but with a deposition time of 2 h leads to increased nanoflake growth as shown in Figure 2S (h).

XRD pattern of G–CNF is compared with that of graphite in Figure 3S (a) in the Supplementary Information. It can be seen that (002) peak of G–CNF at 26.5° is broader

than that of graphite indicating that the interplanar distance between graphene nanosheets is increased and the particles size is decreased. D band and G band of Raman spectrum are shown in Figure 3S (b) confirming graphene formation in our G–CNF sample. Figure 3S (c) shows a photograph of G–CNF dissolved homogenously in water and methanol.

Electrochemical performance

Figure 3a and b shows the CD behavior of Ni–Cu–OH and Ni–Co–OH electrodes of 100:10, respectively. Before 10,000 cycles, there are two separate charging plateaus. The first plateau spans a potential of 0.348 to 0.450 V, while the second plateau spans from 0.450 to 0.532 V. After 10,000 cycles, the first charging plateau is shifted toward higher potential from 0.419 to 0.480 V, while the second plateau covers from 0.480 V to the pre-set maximum charging potential (0.532 V) which is fixed during all 10,000 cycles. This shift in the range of charging plateaus toward higher potentials can be one of the reasons behind the capacitance decay during long CD cycles as confirmed and explained in the following CV results section. In addition, there are two separated discharging plateaus after 10,000 cycles instead of one discharging plateau. Similar CD behavior is also observed for Ni–Co–OH electrode as seen in Fig. 3b, but with one broad plateau in the discharge curve consisting of two or more overlapping plateaus. As expected, both Ni–Cu–OH and Ni–Co–OH electrodes have shorter charging–discharging time after 10,000 cycles, indicating a decrease in capacitance as shown in Fig. 4. All

previous changes in the potential plateau, number of plateaus and shape of charging–discharging curves can be due to structural re-arrangement in the electrode materials as confirmed by CV curves in Fig. 3c and d. CD curves at different current densities of all Ni–Cu–OH and Ni–Co–OH electrodes of 100:3, 100:10 and 100:25 are shown in Figure 4S of the Supplementary Information.

Figure 3c and d illustrates CV behavior of Ni–Cu–OH and Ni–Co–OH electrodes of 100:10, respectively. Before 10,000 cycles, it can be seen in Fig. 3c that there are two partially overlapping oxidation peaks that can be attributed to $\text{Ni}(\text{OH})_2/\text{NiOOH}$ and $\text{Cu}(\text{OH})_2/\text{CuOOH}$ based on the following well-known reactions in which electrons can be stored and then released, reversely:

1. $\text{Ni}(\text{OH})_2 + \text{OH}^- \leftrightarrow \text{NiOOH} + \text{H}_2\text{O} + \text{e}^-$
2. $\text{Cu}(\text{OH})_2 + \text{OH}^- \leftrightarrow \text{CuOOH} + \text{H}_2\text{O} + \text{e}^-$

After 10,000 cycles, the oxidation peak of Ni–Cu–OH electrode is shifted towards higher potential than the initial one of the same electrode. In addition, there are two separated reduction peaks after 10,000 cycles instead of the initial overlapping one. These two observations are in agreement with a similar reported case for $\text{Ni}(\text{OH})_2$

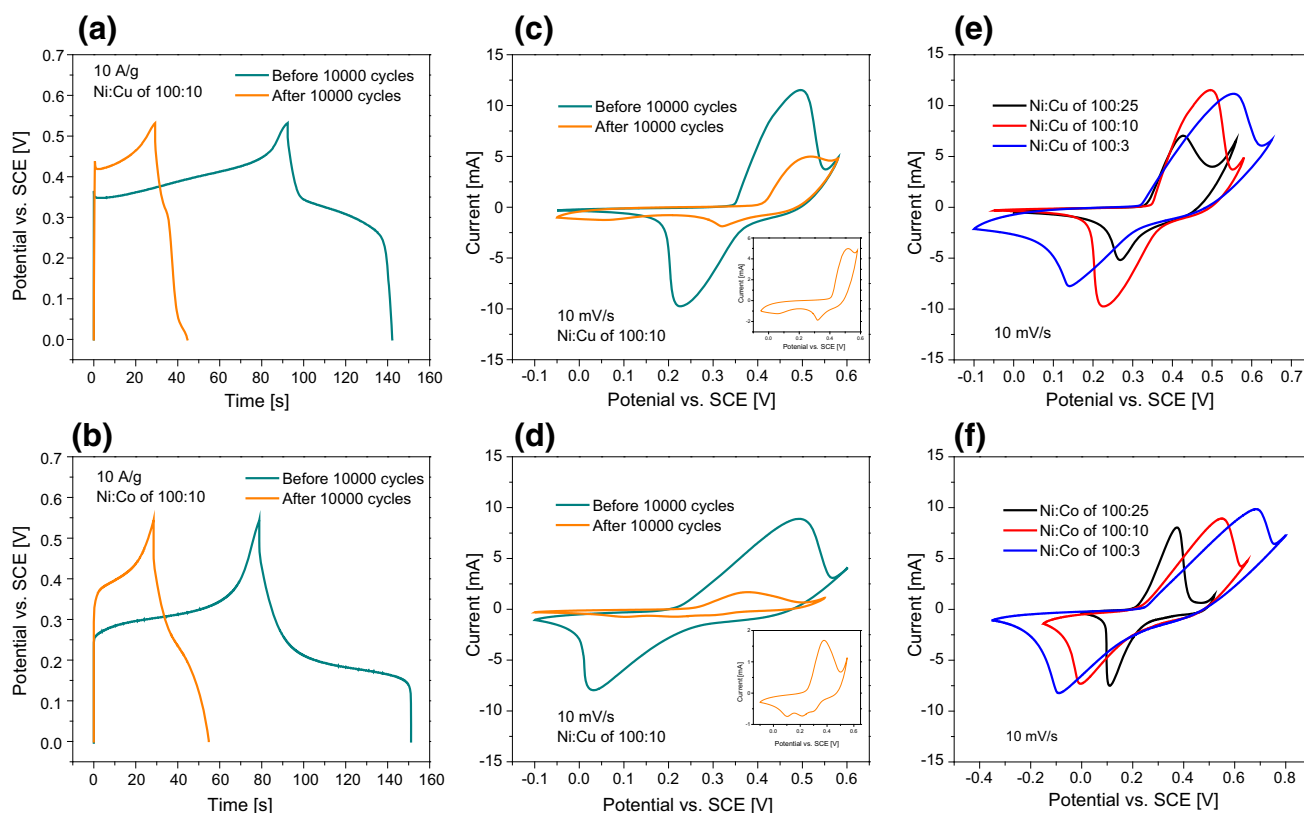


Fig. 3 a, b CD curves of Ni–Cu–OH and Ni–Co–OH electrodes of 100:10, respectively. c, d CV curves of Ni–Cu–OH and Ni–Co–OH electrodes of 100:10, respectively. Enlarged CVs curves after 10,000

cycles are shown in the insets. e, f CV curves of Ni–Cu–OH and Ni–Co–OH electrodes, respectively, of 100:25, 100:10 and 100:3

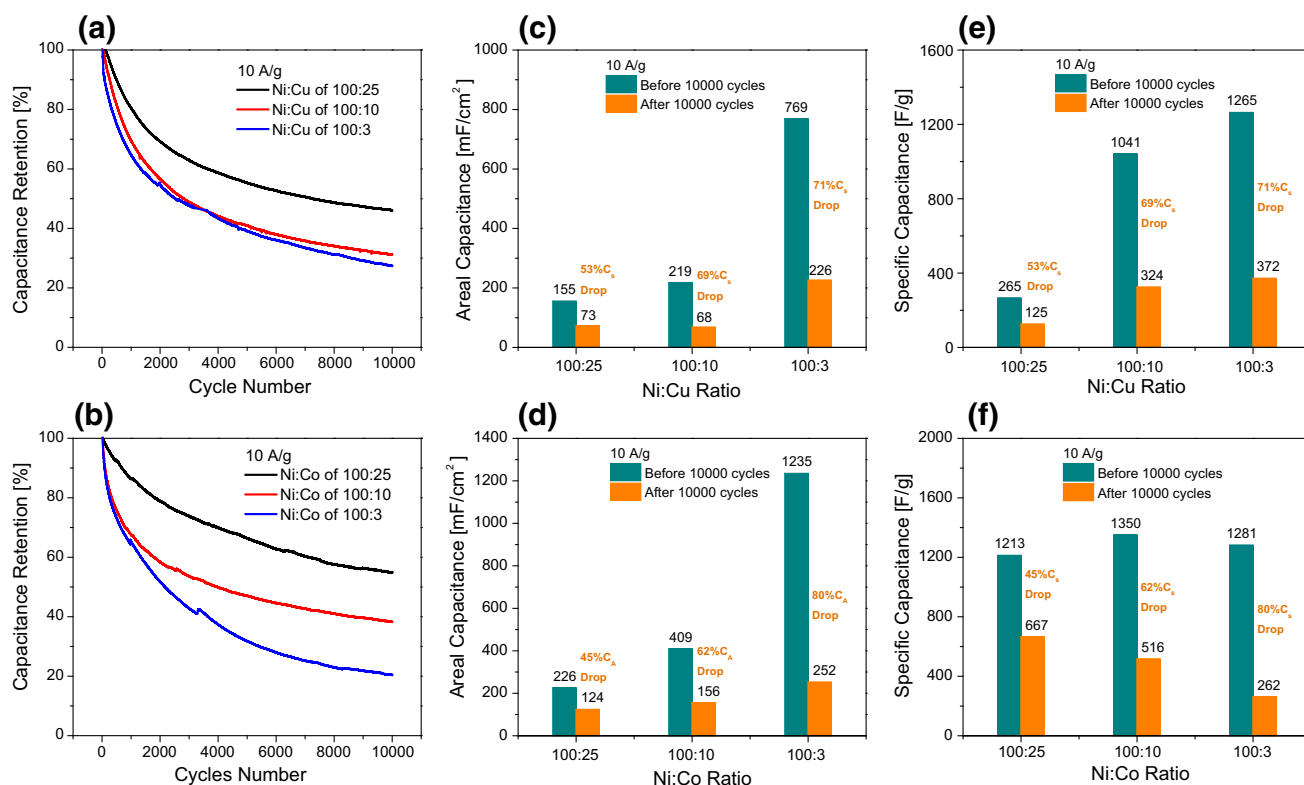


Fig. 4 **a, b** The cycling stability curves of Ni-Cu-OH and Ni-Co-OH electrodes, respectively. **c, d** Areal capacitances of Ni-Cu-OH and Ni-Co-OH electrodes, respectively. **e, f** Specific capacitances of Ni-Cu-OH and Ni-Co-OH electrodes, respectively

electrode [11] and can be explained based on Bode's diagram of the electrochemical phase transformation of nickel hydroxide in alkaline solution [24]. One of the Bode's diagram findings is that the redox potential of β -Ni(OH)₂/ β -NiOOH is higher than that of α -Ni(OH)₂/ γ -NiOOH. Analogous to Bode's diagram, our Ni-Cu-OH electrode may have α -Ni(OH)₂/ γ -NiOOH and α -Cu(OH)₂/ γ -CuOOH-coupled phases in the initial cycles and then they may be transformed to β -Ni(OH)₂/ β -NiOOH and β -Cu(OH)₂/ β -CuOOH-coupled phases due to prolonged cycling in alkaline electrolyte (KOH). Similar CV behavior is also observed for Ni-Co-OH electrode as seen in Fig. 3d. However, three separated reduction peaks are observed after 10,000 cycles, which supports our prediction of the phase transformations from α -Ni(OH)₂/ γ -NiOOH and α -Co(OH)₂/ γ -CoOOH in the initial cycles to β -Ni(OH)₂/ β -NiOOH and β -Co(OH)₂/ β -CoOOH in the final cycles.

Figure 3e and f compares the CVs of Ni-Cu-OH and Ni-Co-OH electrodes, respectively, at the same scan rate of 10 mV/s. Based on the well-generalized relationship stating that smaller potential separation between CV redox peaks indicates higher redox reversibility, it can be concluded that our Ni-Cu-OH electrode of 100:25 has better redox reversibility than Ni-Cu-OH electrodes of 100:10 and 100:3 as indicated by Fig. 3e. Similarly, Ni-Co-OH

electrode of 100:25 has better redox reversibility than Ni-Co-OH electrodes of 100:10 and 100:3 as indicated in Fig. 3f. This redox reversibility seems to lead to better cycling stability of the devices. CVs at different scan rates of all Ni-Cu-OH and Ni-Co-OH electrodes of 100:3, 100:10 and 100:25 are shown in Figure 5S of the Supplementary Information.

Figure 4a and b represents the cycling stability curves of Ni-Cu-OH and Ni-Co-OH electrodes, respectively, of 100:3, 100:10 and 100:25. It can be concluded that using Ni-Cu-OH and Ni-Co-OH electrodes of 100:25 leads to higher capacitance retention during 10,000 CD cycles at 10 A/g, than that of other electrodes of 100:10 and 100:3. This improvement in cycling stability can be ascribed to the characteristic difference in the redox reversibility as indicated by previous CV curves. In addition, Ni-Co-OH electrode of 100:25 exhibits higher capacitance retention of 55 % than 47 % exhibited by Ni-Cu-OH of 100:25, after 10,000 CD cycles at 10 A/g. Areal capacitances of Ni-Cu-OH and Ni-Co-OH electrodes are compared in Fig. 4c and d, respectively, while specific capacitances are compared in Fig. 4e and f for Ni-Cu-OH and Ni-Co-OH electrodes, respectively. As Ni-Cu-OH and Ni-Co-OH electrodes can be used in rechargeable alkaline batteries, areal and specific capacitances are calculated and compared in

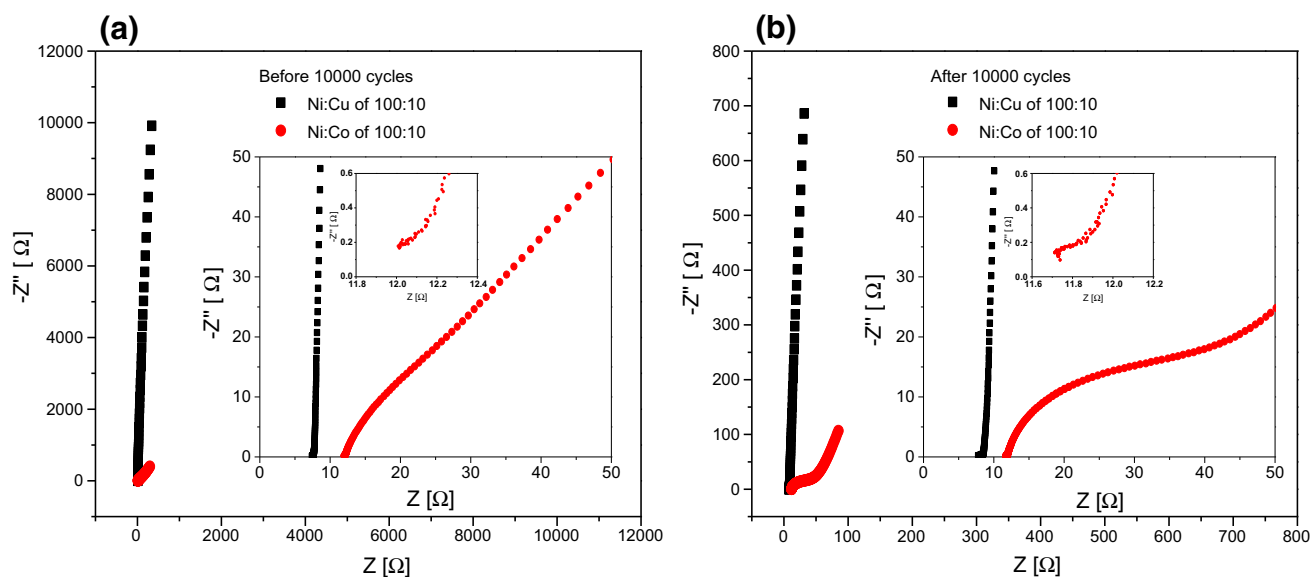


Fig. 5 **a, b** Complex impedance (Nyquist) plots of Ni-Cu-OH and Ni-Co-OH electrodes of 100:10 before and after 10,000 cycles, respectively. Enlarged Nyquist plots are shown in the insets

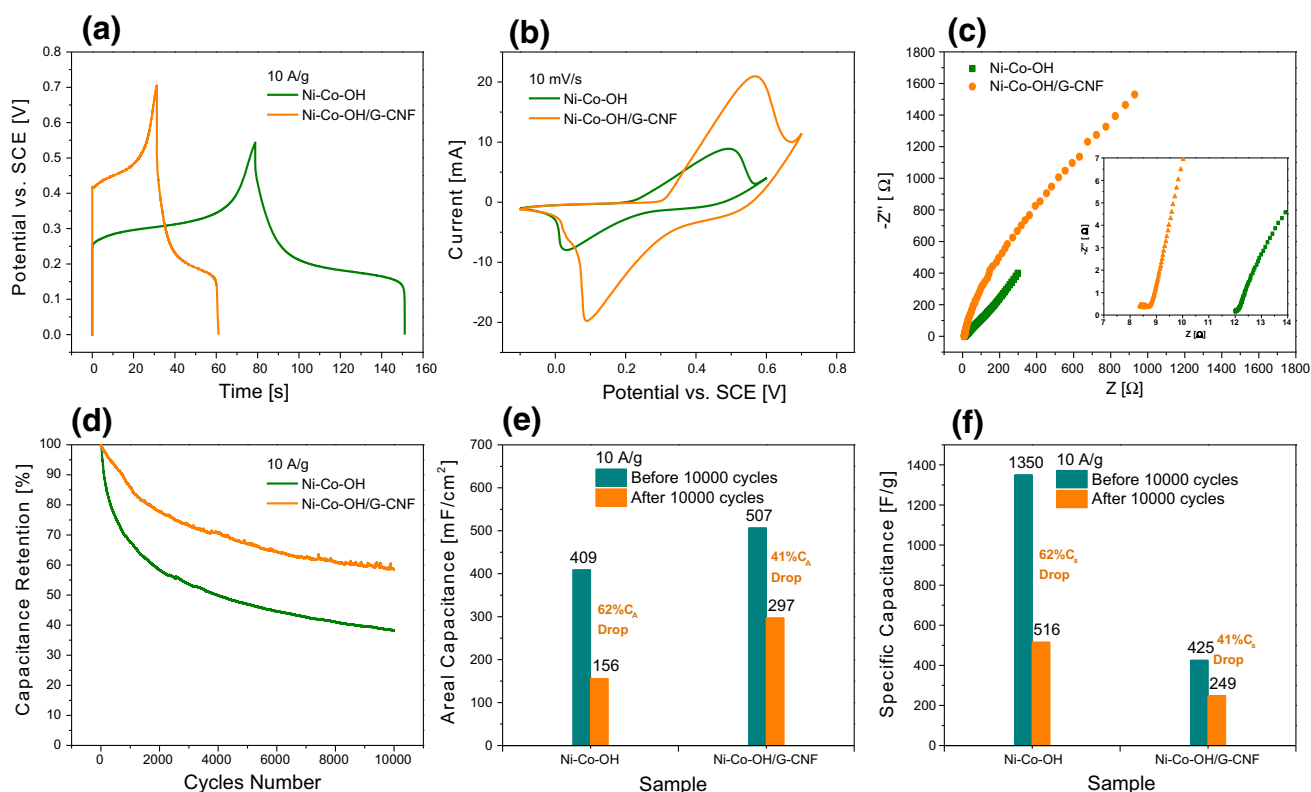


Fig. 6 **a** CD of Ni-Co-OH and Ni-Co-OH/G-CNF electrodes. **b** CV of Ni-Co-OH and Ni-Co-OH/G-CNF electrodes. **c** Nyquist plot of Ni-Co-OH and Ni-Co-OH/G-CNF electrodes. **d** Cycling stability curves of Ni-Co-OH and Ni-Co-OH/G-CNF electrodes. **e, f** Area and specific capacitances of Ni-Co-OH and Ni-Co-OH/G-CNF electrodes, respectively

Figure 6S of the Supplementary Information. Both areal and specific capacitances have been calculated from CD curves of Fig. 4a and b. It is concluded that using Ni-Cu-

plots are shown in the insets. **d** Cycling stability curves of Ni-Co-OH and Ni-Co-OH/G-CNF electrodes. **e, f** Area and specific capacitances of Ni-Co-OH and Ni-Co-OH/G-CNF electrodes, respectively

OH and Ni-Co-OH electrodes 100:3 leads to better areal capacitance than that of other electrodes of 100:10 and 100:25. Such differences in capacitances are expected due

to the different morphologies as shown in previous SEM images. Ni–Co–OH electrode of 100:10 seems to be the optimum composition of our electrode as it has higher capacitance retention than Ni–Cu–OH and Ni–Co–OH electrodes of 100:3 in addition to higher areal and specific capacitances than Ni–Cu–OH and Ni–Co–OH electrodes of 100:25.

Electrochemical impedance spectroscopy results of Ni–Cu–OH and Ni–Co–OH electrodes of 100:10 are represented by the complex impedance (Nyquist) plots in Fig. 5a and b, respectively. At low frequencies, the 45° phase angle of Ni–Co–OH electrode's Nyquist plot represents the presence of Warburg impedance (W) that is due to diffusion of electrolyte ions to the electrode. At high frequencies, Ni–Cu–OH electrode has smaller equivalent series resistance (ESR) than Ni–Co–OH electrode, as can be seen from the x-axis intercept. After 10,000 cycles, the semicircles became more obvious and larger than the initial semicircles. Such increase in charge transfer resistance (R_{CT}) during prolonged cycling is one of the factors behind the decrease in capacitance.

Figure 6 shows the electrochemical performance of Ni–Co–OH/G-CNF electrode compared with the previous Ni–Co–OH electrode of Ni:Co ratio of 100:10. Adding G-CNF to Ni–Co–OH electrode leads to increase potential window as seen in CD and CV curves in Fig. 6a and b, respectively, as expected. Figure 6c of Nyquist plot shows that the ESR of Ni–Co–OH/G-CNF is smaller than that of Ni–Co–OH due to the electrical conductivity of graphene. Moreover, adding G-CNF to Ni–Co–OH electrode leads to enhanced capacitance retention over 10,000 cycles as shown in Fig. 6d. This improvement in the cycling stability can be explained by the fact that there is no phase transformation involved during the charge–discharge process of G-CNF electrode. Figure 6e and f represents areal capacitance and specific capacitance, respectively. Ni–Co–OH/G-CNF electrode has higher areal capacitance (507 mF/cm^2) than Ni–Co–OH electrode (409 mF/cm^2). By taking into account that both electrodes have the same substrate area (1 cm^2), the areal capacitances of these electrodes are actually equivalent to their absolute capacitances. The specific capacitances cannot be measured accurately as shown in Fig. 6f due to the big difference in mass loadings of Ni–Co–OH/G-CNF and Ni–Co–OH. The mass loading of Ni–Co–OH/G-CNF (1.19 mg/cm^2) is 4 times higher than that of Ni–Co–OH (0.30 mg/cm^2) because Ni–Co–OH can be deposited on larger surface area when using G-CNF-carbon microfibers than using only carbon microfibers. As Ni–Co–OH/G-CNF electrode can be used in rechargeable alkaline batteries, areal and specific capacities are calculated and compared in Figure 6S (c) and (f) of the Supplementary Information.

Conclusion

In this project, Ni–Cu–OH and Ni–Co–OH electrodes were prepared using different Ni:Cu and Ni:Co ratios by CBD at room temperature on carbon microfibers. It is observed that incorporation of Co at lower concentration (100:10) enhances nanoflake formation and hence increases capacitance and cycling stability. The improvement in cycling stability can be ascribed to the characteristic difference in the redox reversibility as indicated by CV curves. Phase transformations of Ni–Cu–OH and Ni–Co–OH electrodes are indicated by the shifting and the splitting of CD plateaus and the shifting and the splitting of CV redox peaks. Composites based on the ternary hydroxides, graphene and carbon nanofibers on carbon microfibers increase potential window, decrease equivalent series resistance (ESR), areal capacitance and enhance cycling stability.

Acknowledgments Research reported in this publication was supported by King Abdullah University of Science and Technology (KAUST).

Open Access This article is distributed under the terms of the Creative Commons Attribution 4.0 International License (<http://creativecommons.org/licenses/by/4.0/>), which permits unrestricted use, distribution, and reproduction in any medium, provided you give appropriate credit to the original author(s) and the source, provide a link to the Creative Commons license, and indicate if changes were made.

References

1. BCC Research. Supercapacitors: Technology Developments and Global Markets. Report No. EGY068B. BCC Research (2015). ISBN: 1-62296-035-1
2. Conway, B.E.: Electrochemical Supercapacitors: Scientific Fundamentals and Technological Applications. Springer, New York (1999). doi:[10.1007/978-1-4757-3058-6](https://doi.org/10.1007/978-1-4757-3058-6)
3. Salunkhe, R.R., et al.: Nanoarchitected Graphene-Based Supercapacitors for Next-Generation Energy-Storage Applications. Chem. A Eur. J. **20**, 13838–13852 (2014). doi:[10.1002/chem.201403649](https://doi.org/10.1002/chem.201403649)
4. Faraji, S., Ani, F.N.: The development supercapacitor from activated carbon by electroless plating—a review. Renew. Sustain. Energy Rev. **42**, 823–834 (2015). doi:[10.1016/j.rser.2014.10.068](https://doi.org/10.1016/j.rser.2014.10.068)
5. Augustyn, V., Simon, P., Dunn, B.: Pseudocapacitive oxide materials for high-rate electrochemical energy storage. Energy Environ. Sci. **7**, 1597–1614 (2014). doi:[10.1039/c3ee44164d](https://doi.org/10.1039/c3ee44164d)
6. Faraji, S., Ani, F.N.: Microwave-assisted synthesis of metal oxide/hydroxide composite electrodes for high power supercapacitors—a review. J. Power Source **263**, 338–360 (2014). doi:[10.1016/j.jpowsour.2014.03.144](https://doi.org/10.1016/j.jpowsour.2014.03.144)
7. Feng, L., Zhu, Y., Ding, H., Ni, C.: Recent progress in nickel based materials for high performance pseudocapacitor electrodes. J. Power Source **267**, 430–444 (2014). doi:[10.1016/j.jpowsour.2014.05.092](https://doi.org/10.1016/j.jpowsour.2014.05.092) Review

8. Zhang, K., et al.: Nanostructured Mn-based oxides for electrochemical energy storage and conversion. *Chem. Soc. Rev.* **44**, 699–728 (2015). doi:[10.1039/c4cs00218k](https://doi.org/10.1039/c4cs00218k)
9. Abdelhamid, M.E., O'Mullane, A.P., Snook, G.A.: Storing energy in plastics: a review on conducting polymers and their role in electrochemical energy storage. *RSC Adv.* **5**, 11611–11626 (2015). doi:[10.1039/c4ra15947k](https://doi.org/10.1039/c4ra15947k)
10. Carbonio, R.E., Macango, V.A., Giordano, M.C., Vilche, J.R., Arvia, A.J.: A Transition in the Kinetics of the $\text{Ni}(\text{OH})_2/\text{NiOOH}$ Electrode Reaction. *J. Electrochem. Soc.* **129**, 983–991 (1982). doi:[10.1149/1.2124077](https://doi.org/10.1149/1.2124077)
11. Hu, G., Li, C., Gong, H.: Capacitance decay of nanoporous nickel hydroxide. *J. Power Sources* **195**, 6977–6981 (2010). doi:[10.1016/j.jpowsour.2010.03.093](https://doi.org/10.1016/j.jpowsour.2010.03.093)
12. Kamath, P.V., et al.: Stabilized $\alpha\text{-Ni}(\text{OH})_2$ as Electrode Material for Alkaline Secondary Cells. *J. Electrochem. Soc.* **141**, 2956–2959 (1994). doi:[10.1149/1.2059264](https://doi.org/10.1149/1.2059264)
13. Watanabe, K.-I., Koseki, M., Kumagai, N.: Effect of cobalt addition to nickel hydroxide as a positive material for rechargeable alkaline batteries. *J. Power Sources* **58**, 23–28 (1996). doi:[10.1016/0378-7753\(95\)02272-4](https://doi.org/10.1016/0378-7753(95)02272-4)
14. Chen, J., Bradhurst, D.H., Dou, S.X., Liu, H.K.: Nickel Hydroxide as an Active Material for the Positive Electrode in Rechargeable Alkaline Batteries. *J. Electrochem. Soc.* **146**, 3606–3612 (1999). doi:[10.1149/1.1392522](https://doi.org/10.1149/1.1392522)
15. Liu, B., Zhang, Y., Yuan, H., Yang, H., Yang, E.: Electrochemical studies of aluminum substituted $\alpha\text{-Ni}(\text{OH})_2$ electrodes. *Int. J. Hydrogen Energy* **25**, 333–337 (2000). doi:[10.1016/S0360-3199\(99\)00026-9](https://doi.org/10.1016/S0360-3199(99)00026-9)
16. Jayashree, R.S., Vishnu Kamath, P.: Suppression of the $\alpha \rightarrow \beta$ -nickel hydroxide transformation in concentrated alkali: role of dissolved cations. *J Appl Electrochem* **31**, 1315–1320 (2001). doi:[10.1023/a:1013876006707](https://doi.org/10.1023/a:1013876006707)
17. Lien, C.H., Hu, C.C., Hsu, C.T., Wong, D.S.H.: High-performance asymmetric supercapacitor consisting of Ni–Co–Cu oxyhydroxide nanosheets and activated carbon. *Electrochem. Commun.* **34**, 323–326 (2013). doi:[10.1016/j.elecom.2013.07.032](https://doi.org/10.1016/j.elecom.2013.07.032)
18. Pramanik, P., Bhattacharya, S.: A Chemical Method for the Deposition of Nickel Oxide Thin Films. *J. Electrochem. Soc.* **137**, 3869–3870 (1990). doi:[10.1149/1.2086316](https://doi.org/10.1149/1.2086316)
19. Alhebshi, N.A., Rakhi, R.B., Alshareef, H.N.: Conformal coating of $\text{Ni}(\text{OH})_2$ nanoflakes on carbon fibers by chemical bath deposition for efficient supercapacitor electrodes. *J. Mater. Chem. A* **1**, 14897–14903 (2013). doi:[10.1039/C3TA12936E](https://doi.org/10.1039/C3TA12936E)
20. Sun, X., et al.: Morphology controlled high performance supercapacitor behaviour of the Ni–Co binary hydroxide system. *J. Power Sources* **238**, 150–156 (2013). doi:[10.1016/j.jpowsour.2013.03.069](https://doi.org/10.1016/j.jpowsour.2013.03.069)
21. Zhang, L., Tang, C., Yin, X., Gong, H.: Substrate-assisted self-organization of Ni–Cu spherical double hydroxide (SDH) and its excellent pseudo-capacitive performance. *J. Mater. Chem. A* **2**, 4660–4666 (2014). doi:[10.1039/c3ta14374k](https://doi.org/10.1039/c3ta14374k)
22. Bai, Y., Rakhi, R.B., Chen, W., Alshareef, H.N.: Effect of pH-induced chemical modification of hydrothermally reduced graphene oxide on supercapacitor performance. *J. Power Sources* **233**, 313–319 (2013). doi:[10.1016/j.jpowsour.2013.01.122](https://doi.org/10.1016/j.jpowsour.2013.01.122)
23. An, X., et al.: Stable Aqueous Dispersions of Noncovalently Functionalized Graphene from Graphite and their Multifunctional High-Performance Applications. *Nano Lett.* **10**, 4295–4301 (2010). doi:[10.1021/nl903557p](https://doi.org/10.1021/nl903557p)
24. Bode, H., Dehmelt, K., Witte, J.: Zur kenntnis der nickelhydroxidelektrode—I.Über das nickel (II)-hydroxidhydrat. *Electrochim. Acta* **11**, 1079–1071, doi:[10.1016/0013-4686\(66\)80045-2](https://doi.org/10.1016/0013-4686(66)80045-2) (1966)